OEA | Opto-Electronic Advances

Fast step heterodyne light-induced thermoelastic spectroscopy gas sensing based on a quartz tuning fork with high-frequency of 100 kHz

Yuanzhi Wang†, Ying He†, Shunda Qiao, Xiaonan Liu, Chu Zhang, Xiaoming Duan and Yufei Ma*

https://doi.org/10.29026/oea.2026.250150

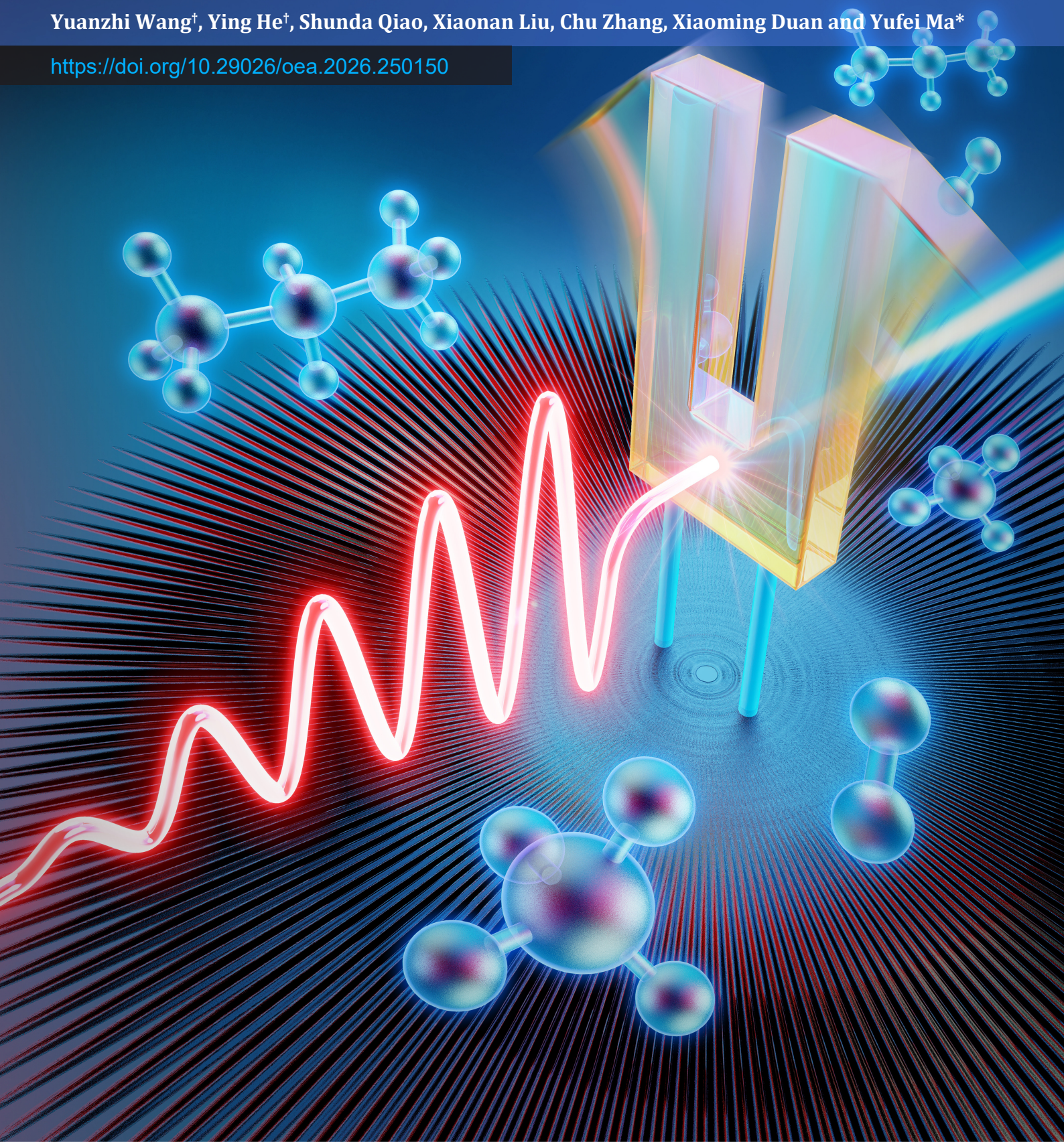

Opto-Electronic Advances

CN 51-1781/TN ISSN (Print) 2096-4579 ISSN (Online) 2097-3993

Fast step heterodyne light-induced thermoelastic spectroscopy gas sensing based on a quartz tuning fork with high-frequency of 100 kHz

Yuanzhi Wang, Ying He, Shunda Qiao, Xiaonan Liu, Chu Zhang, Xiaoming Duan and Yufei Ma*

Citation: Wang YZ, He Y, Qiao SD, Liu XN, Zhang C, Duan XM, Ma YF. Fast step heterodyne light-induced thermoelastic spectroscopy gas sensing based on a quartz tuning fork with high-frequency of 100 kHz. *Opto-Electron Adv* **9**, 250150(2026).

https://doi.org/10.29026/oea.2026.250150

Received: 14 June 2025; Accepted: 28 July 2025; Published online: 28 August 2025

OEA | Opto-Electronic Advances

Article

January 2026, Vol. 9, No. 1

Open Access

Fast step heterodyne light-induced thermoelastic spectroscopy gas sensing based on a quartz tuning fork with high-frequency of 100 kHz

Yuanzhi Wang[1,2†], Ying He[1†], Shunda Qiao[1], Xiaonan Liu[1,2], Chu Zhang[1,2], Xiaoming Duan[1] and Yufei Ma[1,2*]

Abstract: In this paper, a fast step heterodyne light-induced thermoelastic spectroscopy (SH-LITES) sensor using a high-frequency quartz tuning fork (QTF) with resonant frequency of ~100 kHz is reported for the first time. The theoretical principle of heterodyne LITES (H-LITES) signal generation is analyzed firstly, and an acetylene (C_2H_2) H-LITES sensor is established to verify its performance. Experimental comparisons between the high-frequency QTF and a standard commercial QTF with resonant frequency of ~32.768 kHz reveal that the high-frequency QTF exhibits a tenfold faster response time. Specifically, the H-LITES sensor with this QTF achieves a 33 ms measurement cycle, 90% shorter than commercial counterparts. Furthermore, The SH-LITES technique is proposed to further shorten the scanning time to 15 ms, which achieves the shortest LITES measurement time known to date. To demonstrate its advantages in dynamic gas detection, an H_2O-LITES system integrating both QTF types is constructed for real-time monitoring of H_2O concentration during different respiration patterns. Comparative measurements show that the SH-LITES more accurately captures dynamic H_2O concentration fluctuations during respiration, outperforming the commercial QTF-based H-LITES sensor in rapid response scenarios.

Keywords: fast heterodyne light-induced thermoelastic spectroscopy (H-LITES); high-frequency quartz tuning fork (QTF); step heterodyne light-induced thermoelastic spectroscopy (SH-LITES); respiration detection

DOI: 10.29026/oea.2026.250150 | CSTR: 32247.14.oea.2026.250150

Citation: Wang YZ, He Y, Qiao SD et al. Fast step heterodyne light-induced thermoelastic spectroscopy gas sensing based on a quartz tuning fork with high-frequency of 100 kHz. *Opto-Electron Adv* **9**, 250150 (2026).

1 Introduction

Fast and accurate measurement of trace gases is indispensable in various fields including industrial production, healthcare, and environmental monitoring[1–3]. In industrial settings, the combustion process of fuel-air mixtures occurs extremely rapidly, with the entire cycle from injection to complete combustion taking only tens of milliseconds (ms). During this process, the concentrations of oxygen (O_2) and other reactants decrease sharply, while those of products such as carbon dioxide (CO_2) and water vapor (H_2O) rise abruptly[4]. Monitoring of these rapid gas concentration changes can provide insights into the combustion process, aiding in optimizing combustion efficiency[5]. In the healthcare region, fast gas detection allows for dynamic assessment of a patient's respiratory function and physiological state. For instance, during an asthma attack or similar respiratory conditions, the composition of exhaled breath can change within hundreds of ms. Furthermore, respiratory rate serves as a crucial biomarker for assessing a patient's physiological state. Abrupt breathing and changes in respiratory rate can signify a potentially life-threatening deviation in physiological equilibrium[6–9]. These rapidly changing dynamic processes pose challenges for gas detection technology.

Current methods for trace gas detection include optics, electrochemistry, microstructures, and others[10–17]. Among these, spectroscopic techniques are widely researched for their high specificity and sensitivity[18–27]. Quartz-enhanced photoacoustic spectroscopy (QEPAS), introduced in 2002[28],

Received: 14 June 2025

Accepted: 28 July 2025

Published online: 28 August 2025

[1]National Key Laboratory of Laser Spatial Information, Harbin Institute of Technology, Harbin 150000 China; [2]Zhengzhou Research Institute, Harbin Institute of Technology, Zhengzhou 450000, China.
[†]These authors contributed equally to this work.
*Correspondence: YF Ma, E-mail: mayufei@hit.edu.cn

is a notable spectroscopic technique due to its noise resistance, compact size, and cost-effectiveness[29–31]. However, in QEPAS sensor, the detector of quartz tuning fork (QTF) come into direct contact with the measured gases, therefore, it is a contact measurement method and is limited in environments containing acidic or strongly oxidizing gases[32]. To address the limitations of QEPAS, light-induced thermoelastic spectroscopy (LITES) was first introduced in 2018[33]. The principle of LITES involves modulated laser light of specific wavelengths passing through the target gas, which absorbs the laser energy. The transmitted light carries information about the gas concentration and transfers this information to the QTF via thermal expansion[34,35]. The QTF vibrates in response, generating a piezoelectric signal. By demodulating this signal, the concentration of the target gas can be determined[36]. Since LITES measures the transmitted light after absorption, the QTF can be isolated from the measurement environment. This makes it a non-contact method, minimizing environmental interference and ensuring stability[37,38].

Researchers have focused to enhance the detection sensitivity of the QTF. For instance, modifying the dimensions of the QTF changes its deformation degree, thereby increasing the signal amplitude[11,39], and coating materials on the surface of the QTF to enhance the signal amplitude[40–42]. Although QTFs exhibit high detection sensitivity, their response time is limited[43]. In traditional QTF-based QEPAS and LITES technologies, the measurement cycle for gas concentration typically exceeds several seconds[44]. In 2018, a heterodyne signal excitation method was introduced, where an external excitation source causes the laser to rapidly scan across absorption lines, inducing transient response in the QTF at its intrinsic resonant frequency f[45]. Using signal with a frequency of f+Δf to modulate the laser, a beat frequency effect between the intrinsic frequency f and modulation frequency f+Δf can be generated, and the gas concentration and frequency f of QTF can be reconstructed from the demodulated heterodyne signal. However, the measurement cycle based on the beat frequency method still generally exceeds 100 ms, making it unsuitable for dynamic monitoring applications such as combustion fields, respiration, and chemical reactions[46–52].

This paper presents a fast step heterodyne LITES (SH-LITES) sensor using a 100 kHz high-frequency quartz tuning fork (QTF) for the first time. Compared to standard commercial 32 kHz QTFs, the high-frequency QTF offers wider bandwidth, faster energy decay, and shorter response times. The theoretical principle of heterodyne LITES (H-LITES) is analyzed firstly and acetylene (C_2H_2) is used to verify its performance. On the basis of fast H-LITES, SH-LITES is proposed to further reduces the measurement time, establishing the fastest measurement speed among all LITES sensors reported to date. A H_2O sensor combining SH-LITES and H-LITES are built to monitor human respiration states, validating the effectiveness of SH-LITES technique.

2 Operation principle of H-LITES

When a QTF is exposed to a modulated laser in LITES, the performance of the QTF adheres to the damped vibration of a cantilever beam[53,54]. The QTF vibration displacement change x can be expressed by the Eq. (1):

$$m_e\frac{\mathrm{d}^2x}{\mathrm{d}t^2} = -kx - \gamma\frac{\mathrm{d}x}{\mathrm{d}t} + N, \tag{1}$$

where m_e represents the equivalent vibration mass of QTF; k represents the elastic recovery coefficient; γ represents the damping ratio. N represents the driving force generated by the optothermal effect, express by Eq. (2):

$$N = K(I_\lambda + I\cos(2\pi(f+\Delta f)t + \varphi)), \tag{2}$$

where K is the optothermal conversion coefficient; I_λ is transmitted light intensity at the modulated wavelength λ; I is the modulated light intensity; f is the resonant frequency of the QTF. Considering the piezoelectric effect, the input signal to the lock-in amplifier (LIA) is obtained as:

$$\begin{aligned} E_{\mathrm{QTF}}(t) &= R_{\mathrm{eq}}K_{\mathrm{Pe}}(x_0 + x_1 + x_2)\ , \\ x_1 &= X_{\lambda(t)}\cos(2\pi(f+\Delta f)t + \varphi_1)\ , \\ x_2 &= A\mathrm{e}^{-\pi ft/Q}\sin(2\pi ft + \varphi_2)\ , \end{aligned} \tag{3}$$

where R_{eq} is the equivalent resistance; K_{Pe} is the piezoelectric coefficient; x_0 is the bias displacement of the laser irradiation on QTF. x_1 and x_2 are the vibration displacement; f represents the resonant frequency of the QTF, which is primarily determined by its elastic modulus and geometric configuration. Meanwhile, Q denotes the quality factor of the QTF, which is dictated by the material's internal losses and external damping effects[45]. The frequency of reference signal for the LIA is f+Δf. The output $E_{\mathrm{De}}(t)$ after demodulation can be expressed as the Eq. (4):

$$E_{\mathrm{De}}(t) = W_0 + W\cos(2\pi\Delta ft - \varphi_3)\mathrm{e}^{-\pi ft/Q}, \tag{4}$$

where W_0 is proportional to the light intensity I_λ, while W is proportional to the instantaneous variation in I_λ. Therefore, the signal is constituted by the steady-state response and the transient response.

3 Experimental setup

3.1 Verification of H-LITES sensor

The experimental setup of the H-LITES sensor is shown in Fig. 1(a). The laser source is a distributed feedback (DFB) laser with a central output wavelength of ~1530 nm. A sawtooth wave and a sine wave generated by a signal generator are superimposed and injected into the laser controller to achieve wavelength modulation. The first half of the sawtooth wave signal is a ramp signal, used for rapid scanning of the acetylene (C_2H_2) gas absorption line to obtain the gas concentration; the second half is a direct current signal far from the absorption line, used to ensure that the

QTF completely decays the accumulated energy. The sine wave is adopted for modulate the laser wavelength. A fiber collimator (FC) is selected to collimate the light output from the laser. A mixture of 2% C_2H_2 and pure N_2 gas is mixed by a gas flow meter and filled into a 20 cm long gas chamber, where the light is absorbed by C_2H_2. A lens with a focal length of 35 mm focuses the transmitted light onto the surface of the QTF. The piezoelectric signal from the QTF is demodulated using a LIA (Zurich instruments, LIA 500 kHz/5 MHz), with its integration time of 150 μs and its filter order of 3. The demodulated heterodyne signal can reflect the target gas concentration. The experiment uses both high-frequency QTF (QTF1) and standard commercial QTF (QTF2) as detectors. The detailed structural parameters of the two QTFs are shown in Fig. 1(b) and 1(c). It can be observed that the prong structure of QTF1 is shorter in length and wider in width compared to QTF2, resulting in a higher resonant frequency.

The resonant frequencies f of the two QTFs are determined by frequency sweeping using optical excitation, as shown in Fig. 2. The scanning frequency data are fitted with a Lorentz function, yielding a f of 99550 Hz for QTF1 and 32738 Hz for QTF2. The half-maximum bandwidth (ΔW) of the two QTFs are 62 Hz and 5 Hz, respectively. From the formula $Q=f/\Delta W$, the Q values of the QTFs are calculated to be 1605.8 and 6547.6, respectively. A lower Q value indicates greater energy loss in a single vibration cycle of the QTF, suggesting that the QTF can return to a steady state more quickly. Treating the QTF as a filter, the bandwidth of QTF1 is relatively wide, which allows for a greater retention of high-frequency signal components in the input signal. Consequently, the output can more rapidly track changes in the input.

Measurements of the heterodyne signals for both QTFs are conducted under different scan frequencies of sawtooth wave signal. Figure 3(a) shows the heterodyne signal for the QTF1, normalized by the peak signal in 0.25 Hz condition. The reference frequencies f are initially set to 99658 Hz and 32741 Hz for QTF1 and QTF2， respectively. The modulation currents for both are set to 10 mA to ensure that each can generate a heterodyne waveform. At sawtooth wave frequencies of 0.25 Hz and 1 Hz, the scanning speed is rela-

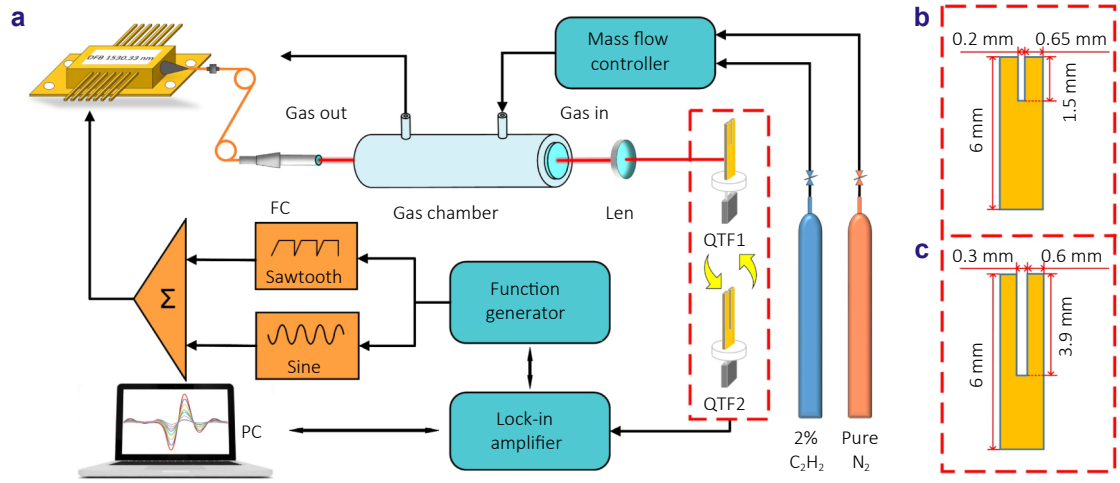

Fig. 1 | (a) Experimental setup of the fast H-LITES sensor based on high-frequency QTF (QTF1) and standard commercial QTF (QTF2). (b) Structure of QTF1. (c) Structure of QTF2.

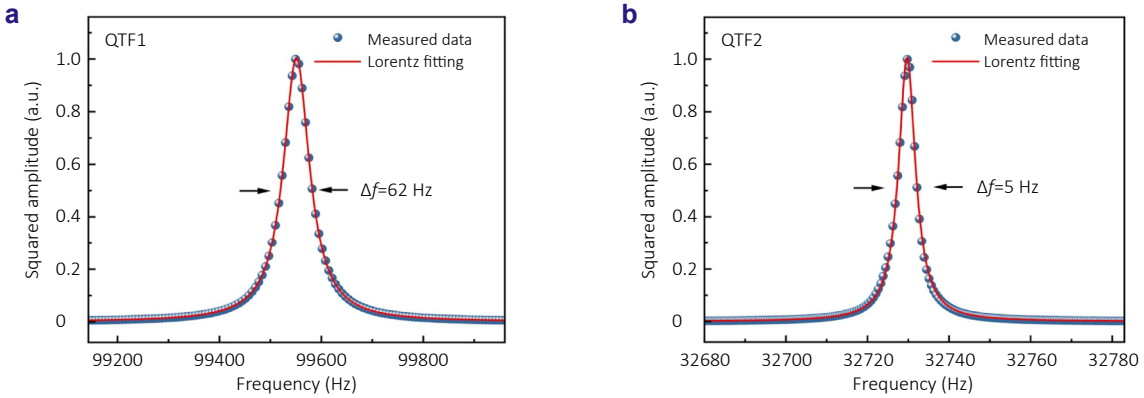

Fig. 2 | Frequency response curve of (a) QTF1; (b) QTF2.

tively slow, leading to a steady-state response from the QTF, resulting in continuous 1*f* harmonic signals. When the sawtooth wave frequency increases to 20 Hz and 30 Hz, the rapid sweep of wavelength across the absorption line causes to the QTF's transient response; the first half of the signal exhibits a 1*f* harmonic, while the latter part displays a multi-peak decay signal. Figure 3(b) illustrates the normalized waveform for the QTF2. At a scan frequency of 1 Hz, the response of the QTF to the excitation already turns into a transient response. When it reaches 20 Hz and 30 Hz, due to the slower energy dissipation of the standard commercial QTF, the QTF2 gets re-excited before it has fully dissipated its previous energy. The interference among different cycles leads to a decrease in the variation of the signal amplitude. Consequently, the shortest measurement period for the heterodyne signal is limited by the decay rate of the QTF's energy.

To determine the minimum measurement period for the two QTFs, their decay processes are fitted based on Eq. (4). The reference frequencies *f* are set to 99702 Hz and 32745 Hz for QTF1 and QTF2, respectively. The waveform of the H-LITES is illustrated in Fig. 4, where the heterodyne signals adequately reflect the decay processes of the two QTFs. The signals exhibit a well-defined exponential decay trend, with *R*-square values reaching 0.999. The t_0 values in the fitting equations are found to be 0.00469 s and 0.04985 s, indicating that the response speed of QTF1 is approximately ten times faster than that of QTF2. The signal attenuation time t_r can be calculated by formula $t_r = \ln(t_0/R)$, where t_0 is the fitted value from Fig. 4, and *R* is the signal attenuation ratio. When the *R* is 0.1%, the attenuation process can be considered almost complete; setting the t_r as the scanning time means there will be no crosstalk between different period. Calculations show that the scanning times of QTF1 and QTF2 are approximately 33 ms and 333 ms, respectively. Based on these times, the sawtooth wave scan frequency can be set to 30 Hz and 3 Hz, respectively, ensuring no interference occurs between heterodyne signals from consecutive scan cycles of the sawtooth wave, thereby maintaining signal integrity and measurement accuracy.

The optimization of the H-LITES peak signal for both QTF1 and QTF2 is conducted to ensure that the signal

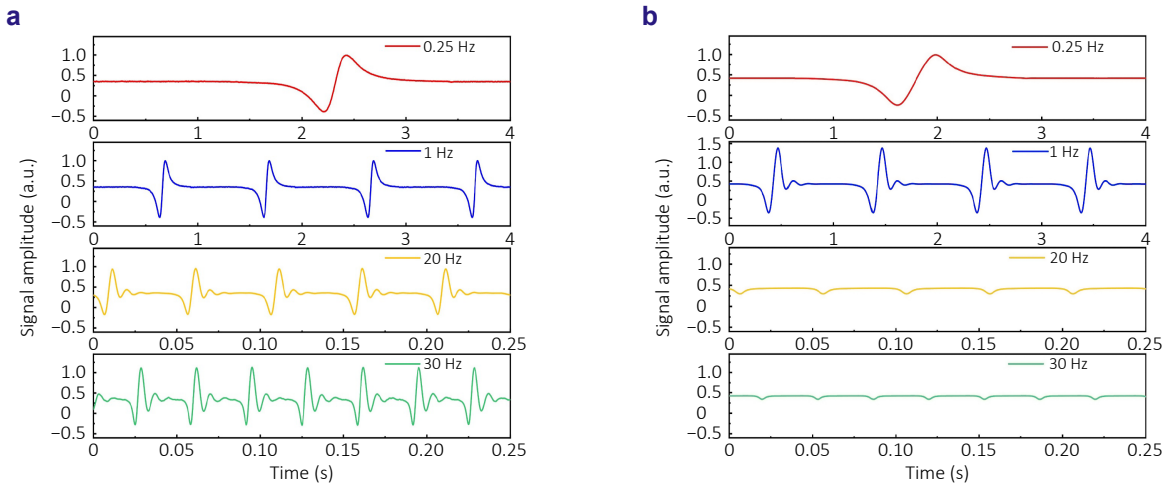

Fig. 3 | Normalized H-LITES signals with different frequencies of sawtooth wave signal: (a) QTF1; (b) QTF2.

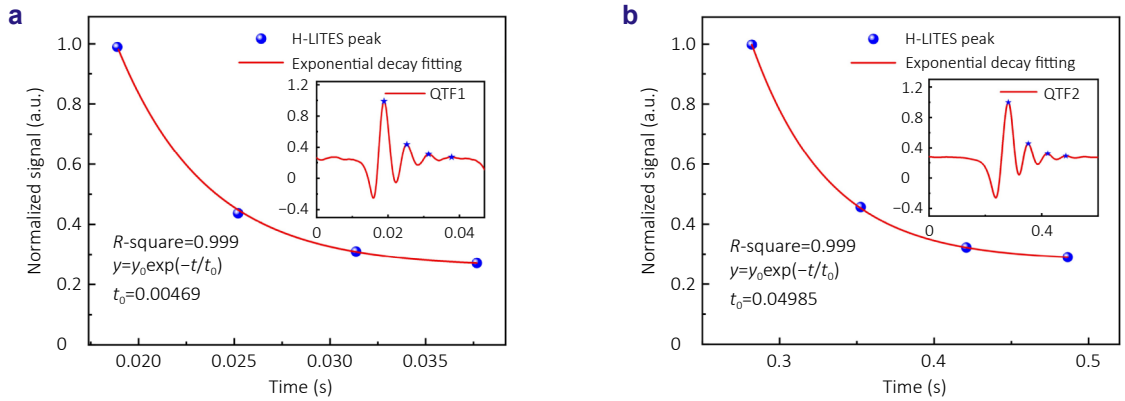

Fig. 4 | The decay curve fitting of QTF in H-LITES sensor: (a) QTF1; (b) QTF2.

amplitudes from both QTFs achieve optimal performance. The variation in modulation depth is shown in Fig. 5(a), indicating that as the modulation current increases, the signal amplitude initially rises before it starts to decrease. The optimal modulation currents for the QTFs are found to be 28 mA and 20 mA. The inconsistency in this modulation current primarily stems from the fact that the laser controller's performance is highly dependent on the modulation frequency. Figure 5(b) and 5(c) illustrates the optimization of the modulation frequency, with the optimal frequencies determined to be 99640 Hz for QTF1 and 32742 Hz for QTF2.

The concentration response of the H-LITES sensor based on the high-frequency QTF1 is investigated. Figure 6(a) presents the H-LITES waveforms at various concentrations of C_2H_2, demonstrating a consistent decrease in the peak-to-peak signal amplitude as the C_2H_2 concentration decreases. Figure 6(b) shows the linear fitting of the peak-to-peak amplitudes at different concentrations, revealing a strong linear relationship between the H-LITES signal and gas concentration, with an *R*-square value of 0.99 for the linear fitting. Based on the positions of peak and valley, the frequency of the QTF can be calibrated. The time difference (Δt) between the peak and trough is 5.65 ms, and $\Delta f = 1/(2\Delta t)$. The calculated Δf is 87.7 Hz. Based on the principle of H-LITES, the calculated resonance frequency of QTF1 is approximately 99552.3 Hz. The discrepancy between this value and the resonance frequency derived from Lorentz fitting is 2.3 Hz, which is significantly smaller than the QTF bandwidth. This outcome demonstrates that H-LITES is capable of fitting the resonance frequency with relatively high accuracy. Therefore, this allows for the calibration of QTF frequency during concentration measurement.

3.2 SH-LITES sensor based on high frequency QTF

To further improve the measurement speed of the LITES system, a step-scan LITES technique (step heterodyne light-induced thermoelastic spectroscopy, SH-LITES) based on high frequency QTF1 is proposed. A comparison of the scanning methods between SH-LITES and H-LITES is shown in Fig. 7. In traditional H-LITES, 1*f* demodulation is typically implemented with a sawtooth wave to scan the absorption line. The leading edge of the sawtooth

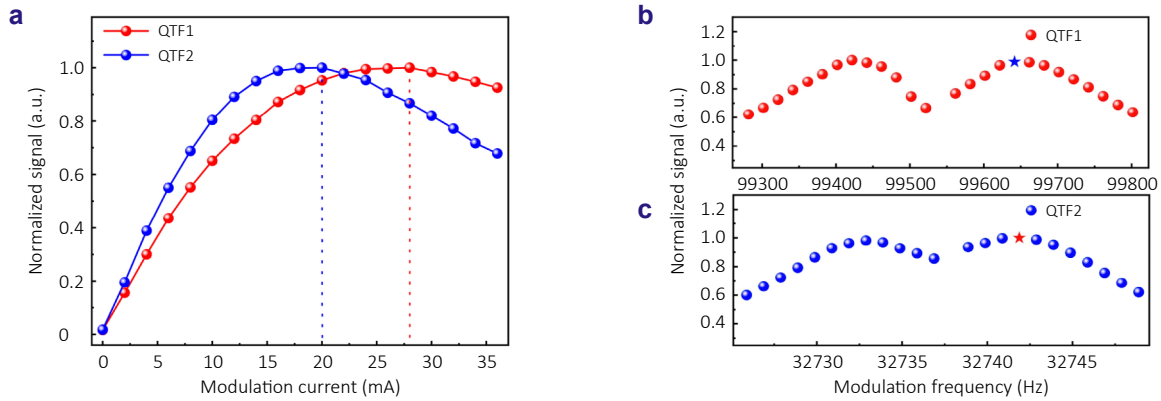

Fig. 5 | Optimization of modulation parameters for H-LITES. (a) Optimization of modulation current. (b) Optimization of modulation frequency for QTF1. (c) Optimization of modulation frequency for QTF2.

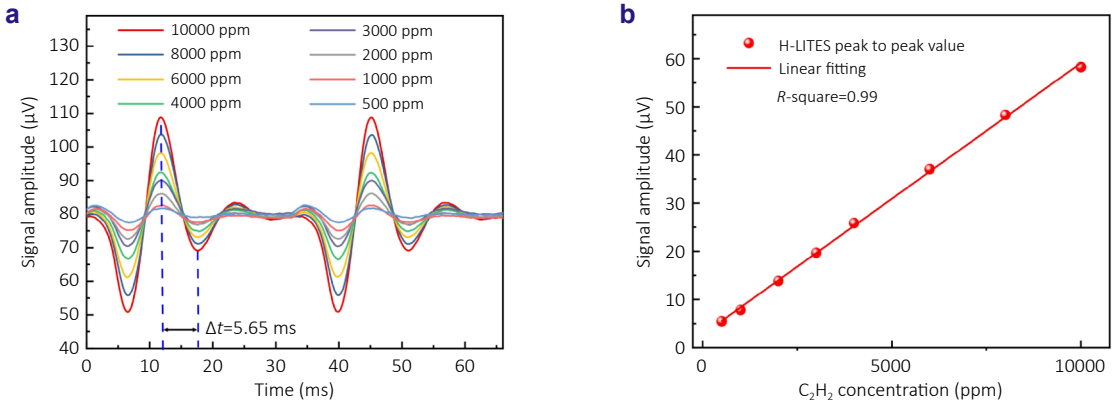

Fig. 6 | H-LITES signals for QTF1 with different concentrations of C_2H_2. (a) Signals with different C_2H_2 concentration. (b) Linear fitting of peak to peak value of the signal.

wave sweeps the laser wavelength across the entire target absorption line. In LITES, the 1*f* signal originates from periodic temperature fluctuations induced by optical absorption, which in turn excites the vibration of a QTF. According to the differential characteristics of absorption spectra, the 1*f* signal amplitude is proportional to the first derivative of the absorption coefficient. Its peaks correspond to the positions with the maximum slope of the absorption line, whereas scanning the absorption line center (where the slope is zero) and baseline regions (with no absorption) generates no effective signals. In practice, signal amplitudes reflecting gas concentration only emerge at the two peaks of the 1*f* signal, making wavelength scanning at other positions unnecessary. SH-LITES performs scanning only near the two 1*f* peaks, avoiding scans of invalid positions and shortening the measurement period without altering the QTF response time, and after traversing a small range, the current is abruptly switched near the other peak. The resulting current jump generates heterodyne signals, which can reflect the frequency difference Δ*f*.

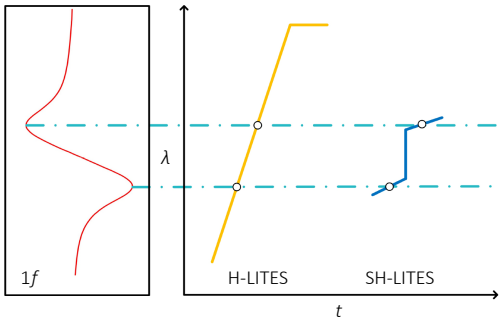

Fig. 7 | Comparison of scanning methods between H-LITES and SH-LITES.

The amplitude of the modulation waveform is optimized in the experiment. As shown in the Fig. 8, the scan current amplitude is determined to be 2.2 mA, and the step current amplitude is 11 mA.

The optimization of modulation frequency and current is shown in Fig. 9. The SH-LITES modulation waveform is optimized under a 33 ms scanning period. As depicted in

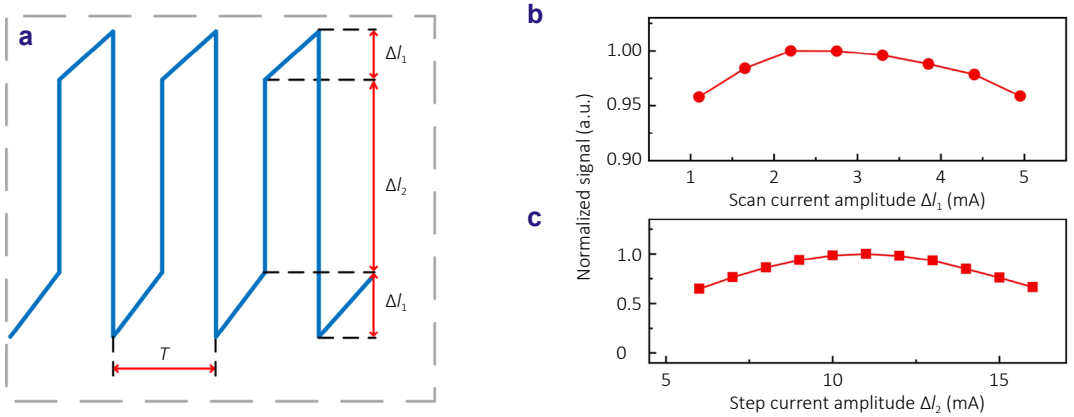

Fig. 8 | Optimization of the scan waveform for SH-LITES. (a) Illustration of step-scan wave. (b) Optimization of scan current ΔI_1. (c) Optimization of scan current ΔI_2.

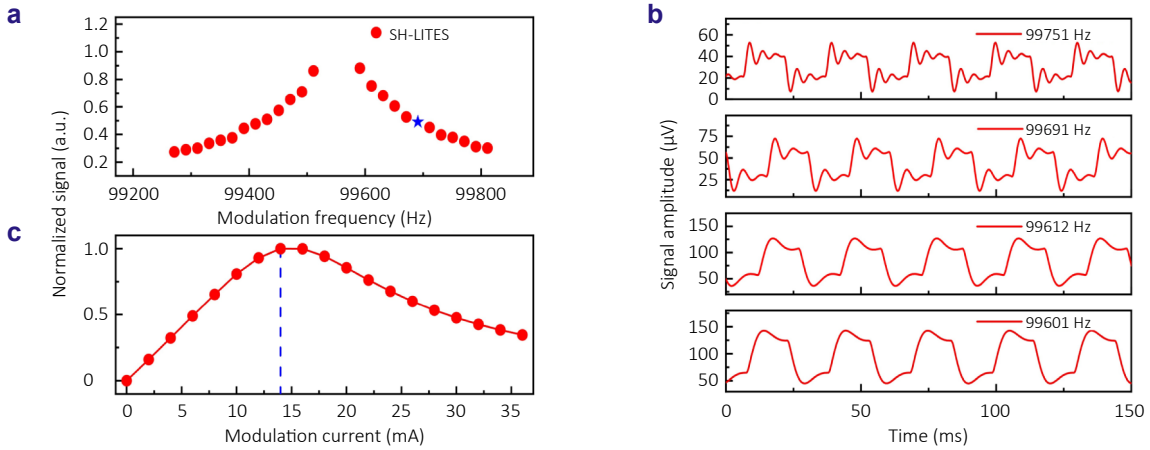

Fig. 9 | Optimization of modulation parameters for SH-LITES. (a) Optimization of modulation frequency. (b) SH-LITES waveform with different modulation frequency. (c) Optimization of modulation current.

Fig. 9(a) and 9(b), the signal amplitude and waveforms at different modulation frequencies reveal that the closer the modulation frequency approaches the QTF's resonance frequency, the larger the signal amplitude becomes. However, the heterodyne valley gradually disappears, resulting from the increase in Δt. To ensure the heterodyne waveform can calibrate the QTF frequency under shorter scanning periods, the modulation frequency is set to 99691 Hz in subsequent experiments instead of the frequency with the maximum signal amplitude. At this point, the calculated Δf is 141 Hz. From the formula $\Delta t = 1/(2\Delta f)$, the value of Δt is 3.55 ms. When the scanning period is greater than twice Δt, the existence of the valley can be maintained, thereby inverting the QTF frequency. The curve of signal amplitude versus modulation current is shown in Fig. 9(c), determining the optimal modulation current as 14 mA.

When comparing the optimized signal amplitudes of SH-LITES and H-LITES across different scanning periods, as is depicted in Fig. 10, their correlation with the period reveals distinct behaviors. H-LITES signals decay rapidly as the period shortens. This decay originates from insufficient baseline scanning duration, which induces crosstalk of vibrational energy. In contrast, SH-LITES signals exhibit no continuous decay within this range. Specifically, at a 15 ms scanning period, the SH-LITES amplitude reaches 57.7 μV, closely approaching the 54.2 μV amplitude of H-LITES at 33 ms. Thus, the scanning period can be reduced to half that of H-LITES, demonstrating the temporal efficiency advantage of stepwise scanning.

The linear concentration response of SH-LITES is measured under a 15 ms scanning period, as shown in Fig. 11. Specifically, signal amplitudes are monitored as the C_2H_2 concentration ranged from 500 to 10000 ppm, demonstrating an excellent linear response with an *R*-square value of 0.99. During the decay process, the time difference (Δt = 3.58 ms) and frequency difference (Δf = 139.7 Hz) between peak and valley positions are calculated to retrieve the QTF resonance frequency. The 1.3 Hz difference between the value calculated by SH-LITES and that obtained via Lorentz fitting indicates that SH-LITES in a period of 15 ms can still calibrate the QTF frequency, leveraging precise heterodyne waveform analysis.

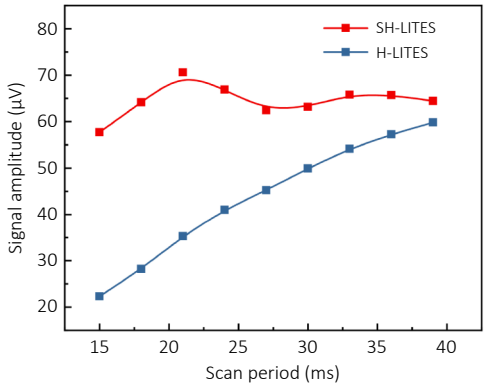

Fig. 10 | Signal comparison between SH-LITES and H-LITES under various scanning periods.

3.3 H_2O respiration detection based on the fast SH-LITES sensor

To further validate the advantages of fast SH-LITES sensor based on QTF1 for rapid measurements, H_2O respiration detection is demonstrated. The experimental setup is illustrated in Fig. 12(a). QTF2 is also employed for comparison. Two lasers with central wavelengths near the absorption line of H_2O at 1368 nm are employed. Wavelength modulation is achieved by applying sine waves of different frequencies to each laser. To implement SH-LITES, a step-scan waveform is applied to laser1, which illuminates QTF1. To demonstrate the advantages of SH-LITES technology, H-LITES technology is also used to measure H_2O respiration. Therefore, laser2 and QTF2 are adopted in this H-LITES sensor. The output beams from the two lasers pass through the same gas chamber and are focused by lenses onto QTF1 and

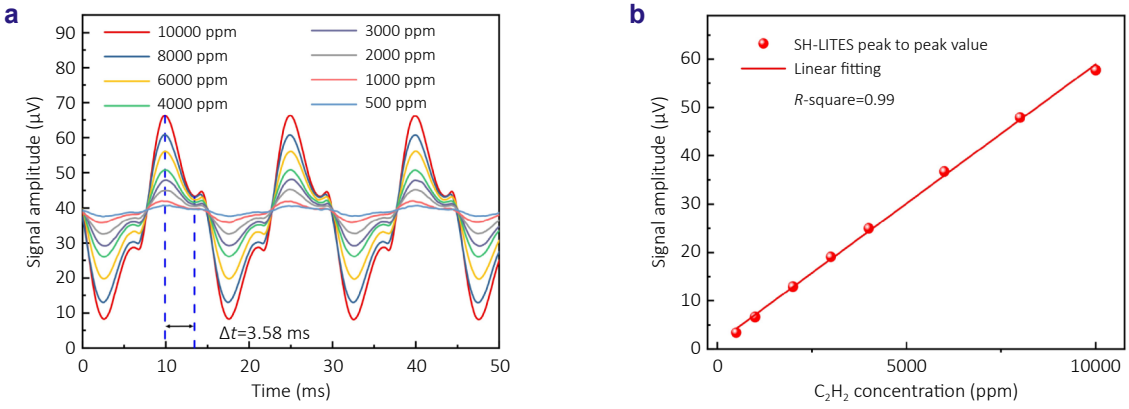

Fig. 11 | SH-LITES for QTF1 with different concentrations of C_2H_2. (a) Signals with different C_2H_2 concentration. (b) Linear fitting of peak to peak value of the signal.

QTF2, respectively. Two channels of the LIA are used to demodulate the signals from the QTFs, thereby obtaining the SH-LITES and H-LITES signals. The gas chamber is designed with openings at both ends to remain connected to the external environment, as shown in Fig. 12(b), ensuring a constant pressure inside the cell. The length of the gas cell is 20 cm and the inner diameter is 2 cm. The air chamber has an opening in its middle section and is connected to the breathing mouthpiece via a rubber tube. When the experimenter breathes through the mouthpiece, the exhaled gas fills the entire air chamber, thereby altering the H_2O concentration along the laser path. The signals demodulated by the LIA are processed by a computer to determine the variations in H_2O concentration, thereby reflecting the state of respiration. The experiment is conducted under the conditions of 21 °C and 101 kPa. Sine waves of 99702 Hz and 32745 Hz are applied initially to the respective lasers. Based on the earlier research about SH-LITES and H-LITES, the frequency of step-scan wave and sawtooth wave signal are set to 3 Hz and 66.67 Hz, corresponding to the shortest measurement periods, respectively. The two channels of the LIA use the same integration time and filter order as before.

The optical path is adjusted so that the laser beam irradiated the optimal position of the QTFs, after which the modulation frequency and modulation current is optimized. Figure 13(a) and 13(b) illustrates the optimization of the modulation frequency, with the optimal frequencies determined to be 99655 Hz for QTF1 and 32748 Hz for QTF2. The optimization of the modulation current is illustrated in Fig. 13(c) and 13(d), where the optimal modulation current for QTF1 and QTF2 are found to be 24 mA and 34 mA, respectively. Since the absorption linewidth of H_2O differs from that of C_2H_2, the scan current amplitude and the step current amplitude are also optimized, determined to be 1 mA and 10 mA, respectively.

The SH-LITES sensor and H-LITES sensor are employed for continuous measurement of H_2O in the gas chamber. The experiment measures H_2O in the air, as well as under three breathing conditions: normal breathing, fast breathing, and slow breathing. The obtained results using QTF1 and QTF2 are shown in Fig. 14. Due to the significantly shorter scanning period of SH-LITES with QTF1 compared to H-LITES with QTF2, the sampling rate for H_2O concentration is much higher. Consequently, the obtained signal envelope is more continuous. The peak-to-peak values of the LITES sensor signals in Fig. 14 are extracted to obtain signal wave-

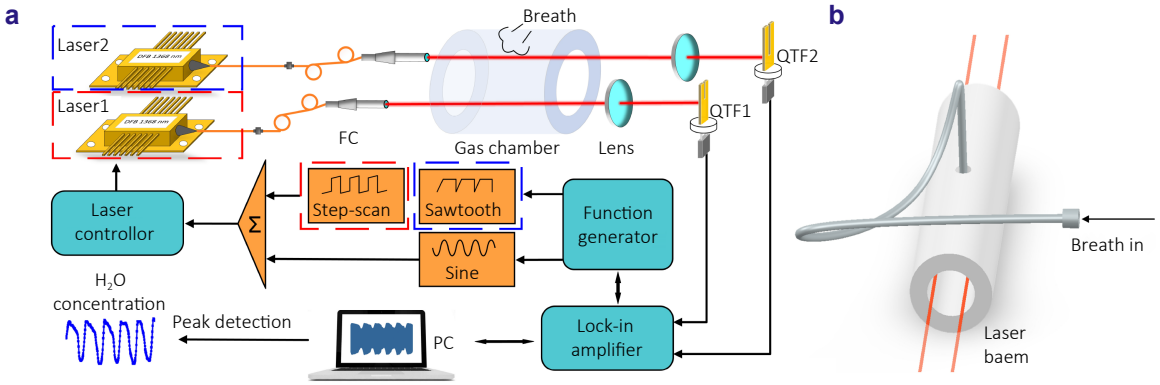

Fig. 12 | (a) Experimental setup of H_2O-H-LITES sensor for respiration detection. (b) Schematic diagram of the gas chamber.

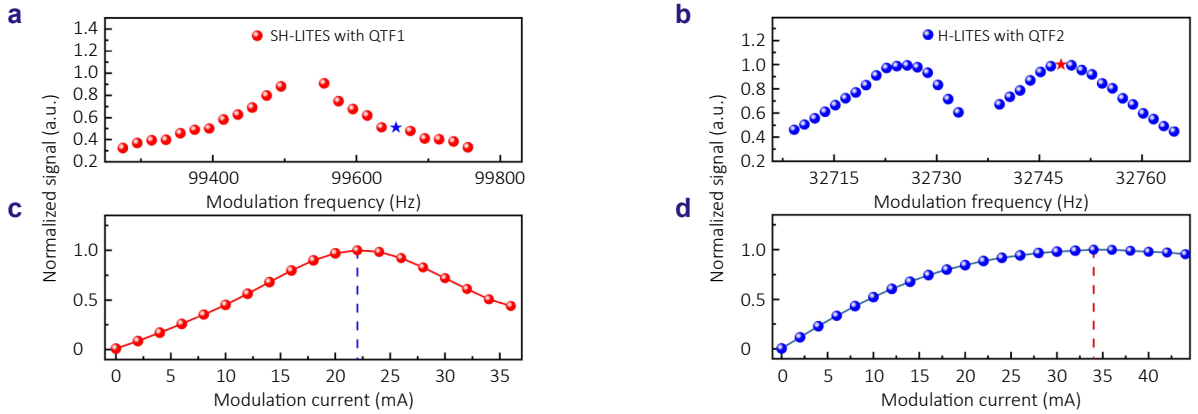

Fig. 13 | Optimization of modulation parameters. Optimization of modulation frequency for (a) SH-LITES with QTF1; (b) H-LITES with QTF2. Optimization of modulation current for (c) SH-LITES with QTF1; (b) H-LITES with QTF2.

forms that reflect changes in H_2O concentration. In Fig. 15(a) and 15(b), the H_2O concentration for QTF1 and QTF2 are illustrated respectively. Measurements of H_2O in the air indicate that the SH-LITES and H-LITES system both possess good stability over a certain period of time. Under normal and slow breathing conditions, both QTFs are capable of reflecting the overall trend of respiration. However, the waveform of SH-LITES with QTF1 reveals more details in the breathing process compared to H-LITES with QTF2. In the state of fast breathing, the waveform of QTF2 becomes distorted and fails to reflect the correct respiratory frequency. In contrast, the waveform of QTF1 still manages to accurately reflect changes in the respiratory state. This demonstrates that SH-LITES with QTF1 is more suitable than H-LITES with QTF2 for scenarios involving rapid changes in gas concentration. The scan time and related parameters of SH-LITES sensor based on the high-frequency QTF1 are compared to the other LITES sensors, and the results are presented in Table 1. Results show that the SH-LITES sensor with high-frequency QTF1 has significantly improved the measurement speed.

4 Conclusions

This paper reports for the first time a fast SH-LITES sensor leveraging a high-frequency QTF with a resonant frequency of ~100 kHz. The theoretical mechanism of H-LITES is analyzed, followed by the establishment of a C_2H_2-H-LITES sensor to compare the response speeds of the high-frequency QTF and a standard commercial QTF. Experimental results demonstrate that the high-frequency QTF exhibits a tenfold faster response speed and a 33 ms mea-

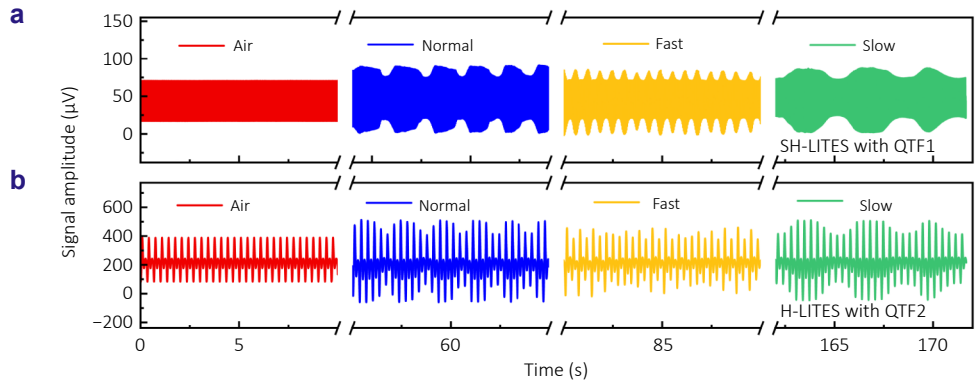

Fig. 14 | H_2O-LITES sensor signal amplitude recorded as a function of time for human respiration: (a) SH-LITES with QTF1; (b) H-LITES with QTF2.

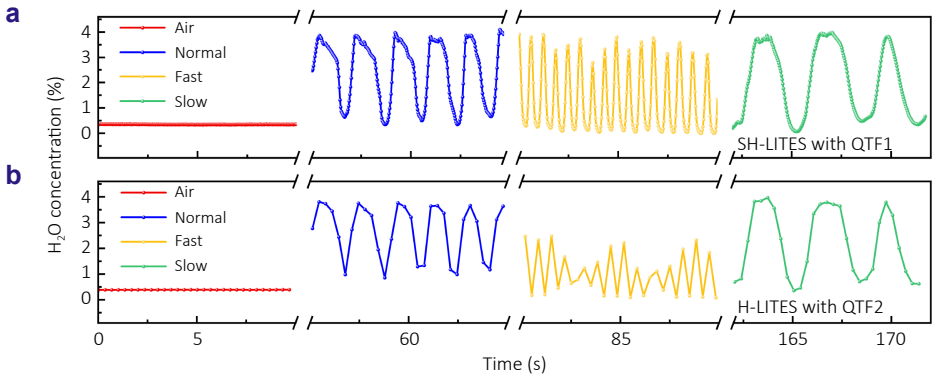

Fig. 15 | H_2O concentration obtained by peak-to-peak extraction of SH-LITES and H-LITES sensor: (a) SH-LITES with QTF1; (b) H-LITES with QTF2.

Table 1 | Parameter comparison of measurement speeds with other LITES sensors.

Technique	QTF frequency (kHz)	Intergration time (ms)	Measurement period (s)	Reference
LITES	9	240	100	ref.[34]
LITES	32	100	10	ref.[55]
LITES	32	30	5	ref.[56]
H-LITES	9	30	4	ref.[48]
SH-LITES	100	0.15	0.015	This work

surement period compared to the commercial counterpart, attributed to its broader bandwidth. To further minimize the measurement cycle, a SH-LITES method based on step waveform scanning is proposed, which currently represents as the fastest LITES sensor with a measurement cycle of just 15 ms. Additionally, a fast H_2O-SH-LITES sensor is developed for real-time H_2O measurement in respiration. Comparative studies between the SH-LITES and H-LITES show that the SH-LITES accurately captures respiration frequency and state changes, even during rapid breathing. Its advantage in dynamic scenarios with rapid gas concentration fluctuations offers a promising direction for enhancing the measurement speed of QTF-based spectroscopic gas sensors, particularly in biomedical monitoring and environmental rapid detection.

References

1. Yuan ZY, Lou XT, Chu Q et al. Ultrarapid spectroscopic gas detection via frequency-agile and compressed sensing. *Appl Phys B* **128**, 66 (2022).
2. Liu CY, Gu YM, Liu C et al. Missing-linker 2D conductive metal organic frameworks for rapid gas detection. *ACS Sens* **6**, 429–438 (2021).
3. Dong Y, Duan SK, Long SY et al. Ultrasensitive and fast gas detection based on room-temperature indium arsenide mid-wavelength infrared photodetectors. *Adv Funct Mater* **35**, 2422398 (2025).
4. Li CN, He Y, Qiao SD et al. A low-cost full-range hydrogen sensor based on quartz tuning fork. *IEEE Sens J* **25**, 16943–16949 (2025).
5. Hong JW, Kim Y, Yoon SH et al. Simultaneous measurement of temperature, concentration, and velocity in the combustion field using TDLAS. *J Mech Sci Technol* **37**, 5199–5206 (2023).
6. Tanneberger T, Schimek S, Paschereit CO et al. Combustion efficiency measurements and burner characterization in a hydrogen-oxyfuel combustor. *Int J Hydrogen Energy* **44**, 29752–29764 (2019).
7. Tong A, Baumgart A, Evangelidis N et al. Core outcome measures for trials in people with coronavirus disease 2019: respiratory failure, multiorgan failure, shortness of breath, and recovery. *Crit Care Med* **49**, 503–516 (2021).
8. Ye LX, Wu F, Xu RX et al. Face mask integrated with flexible and wearable manganite oxide respiration sensor. *Nano Energy* **112**, 108460 (2023).
9. Endoh H, Yamaguchi S, Hayashi Y et al. Variability of respiratory rate or heart rate reflects degree of organ dysfunction in sepsis. *Crit Care Med* **41**, A141 (2013).
10. Ma HX, Qiao SD, He Y et al. Load capacitance matching for resonant frequency adjusting-based multi-quartz tuning fork-enhanced laser spectroscopic sensing. *Opt Express* **33**, 9423–9433 (2025).
11. Wang RQ, Qiao SD, He Y et al. Highly sensitive laser spectroscopy sensing based on a novel four-prong quartz tuning fork. *Opto-Electron Adv* **8**, 240275 (2025).
12. Jiang GP, Goledzinowski M, Comeau FJE et al. Electrochemical gas sensors: free-standing functionalized graphene oxide solid electrolytes in electrochemical gas sensors (Adv. Funct. Mater. 11/2016). *Adv Funct Mater* **26**, 1670 (2016).
13. Jiang SL, Chen FF, Zhao Y et al. Broadband all-fiber optical phase modulator based on photo-thermal effect in a gas-filled hollow-core fiber. *Opto-Electron Adv* **6**, 220085 (2023).
14. Shao MR, Ji C, Tan JB et al. Ferroelectrically modulate the fermi level of graphene oxide to enhance SERS response. *Opto-Electron Adv* **6**, 230094 (2023).
15. Shi LY, Li YJ, Li Z. Early cancer detection by SERS spectroscopy and machine learning. *Light Sci Appl* **12**, 234 (2023).
16. Ma HX, Sun XR, Qiao SD et al. A high-performance light-induced thermoelastic spectroscopy sensor based on a high-Q value quartz tuning fork load. *Sens Actuator B Chem* **436**, 137713 (2025).
17. Qiu XB, Xiong XH, Li L et al. Development of an FDM-TDLAS sensor for long-term online monitoring of H_2S and CO to predict water wall corrosion trends. *Anal Chem* **97**, 14058–14066 (2025).
18. Sun HY, He Y, Qiao SD et al. Highly sensitive H_2S-LITES sensor with 80 m fiber-coupled multi-pass cell based on optical path multiplexing technology. *Photoacoustics* **42**, 100699 (2025).
19. Xu BX, Wan YY, Fan XY et al. Whispering-gallery-mode barcode-based broadband sub-femtometer-resolution spectroscopy with an electro-optic frequency comb. *Adv Photonics* **6**, 016006 (2024).
20. Sun XR, Sun HY, He Y et al. An ultrahighly sensitive CH_4-TDLAS sensor based on an 80-m optical path length multipass cell with a dense circular spot pattern. *Anal Chem* **97**, 10886–10892 (2025).
21. Nie QX, Peng YB, Chen QH et al. Agile cavity ringdown spectroscopy enabled by moderate optical feedback to a quantum cascade laser. *Opto-Electron Adv* **7**, 240077 (2024).
22. Hou JF, Liu XN, Sun HY et al. Dual-component gas sensor based on light-induced thermoelastic spectroscopy and deep learning. *Anal Chem* **97**, 5200–5208 (2025).
23. Wang XY, Qiu XK, Liu ML et al. Flat soliton microcomb source. *Opto-Electron Sci* **2**, 230024 (2023).
24. Wang YQ, Zhang JH, Zheng YC et al. Brillouin scattering spectrum for liquid detection and applications in oceanography. *Opto-Electron Adv* **6**, 220016 (2023).
25. Zhang C, He Y, Qiao SD et al. High-sensitivity trace gas detection based on differential Helmholtz photoacoustic cell with dense spot pattern. *Photoacoustics* **38**, 100634 (2024).
26. Fu BT, Gao RH, Yao N et al. Soliton microcomb generation by cavity polygon modes. *Opto-Electron Adv* **7**, 240061 (2024).
27. Ma J, Fan EB, Liu HJ et al. Microscale fiber photoacoustic spectroscopy for in situ and real-time trace gas sensing. *Adv Photonics* **6**, 066008 (2024).
28. Kosterev AA, Bakhirkin YA, Curl RF et al. Quartz-enhanced photoacoustic spectroscopy. *Opt Lett* **27**, 1902–1904 (2002).
29. Ma YF, Qiao SD, Wang RQ et al. A novel tapered quartz tuning fork-based laser spectroscopy sensing. *Appl Phys Rev* **11**, 041412 (2024).
30. Zifarelli A, Negro G, Mongelli LA et al. Effect of gas turbulence in quartz-enhanced photoacoustic spectroscopy: a comprehensive flow field analysis. *Photoacoustics* **38**, 100625 (2024).
31. Qiao SD, He Y, Sun HY et al. Ultra-highly sensitive dual gases detection based on photoacoustic spectroscopy by exploiting a long-wave, high-power, wide-tunable, single-longitudinal-mode solid-state laser. *Light Sci Appl* **13**, 100 (2024).
32. Zifarelli A, Sampaolo A, Patimisco P et al. Methane and ethane detection from natural gas level down to trace concentrations using a compact mid-IR LITES sensor based on univariate calibration. *Photoacoustics* **29**, 100448 (2023).
33. Ma YF, He Y, Tong Y et al. Quartz-tuning-fork enhanced photothermal spectroscopy for ultra-high sensitive trace gas detection. *Opt Express* **26**, 32103–32110 (2018).
34. Liu YH, Qiao SD, Fang C et al. A highly sensitive LITES sensor based on a multi-pass cell with dense spot pattern and a novel quartz tuning fork with low frequency. *Opto-Electron Adv* **7**, 230230 (2024).
35. Ma YF, Liang TT, Qiao SD et al. Highly sensitive and fast hydrogen detection based on light-induced thermoelastic spectroscopy. *Ultrafast Sci* **3**, 0024 (2023).
36. Sun HY, He Y, Qiao SD et al. Highly sensitive and real-simultaneous CH_4/C_2H_2 dual-gas LITES sensor based on Lissajous pat-

tern multi-pass cell. *Opto-Electron Sci* **3**, 240013 (2024).
37. He Y, Wang YZ, Qiao SD et al. Hydrogen-enhanced light-induced thermoelastic spectroscopy sensing. *Photonics Res* **13**, 194–200 (2025).
38. Sun HY, Liu YH, He Y et al. Highly sensitive CH_4/C_2H_2 dual-gas light-induced thermoelastic spectroscopy sensor based on a dual-path multiring multipass cell and a circle-head quartz tuning fork. *ACS Sens* **10**, 4717–4724 (2025).
39. Wang LH, Lv HH, Zhao YH et al. Sub-ppb level HCN photoacoustic sensor employing dual-tube resonator enhanced clamp-type tuning fork and U-net neural network noise filter. *Photoacoustics* **38**, 100629 (2024).
40. Lou CG, Li XT, Chen HJ et al. Polymer-coated quartz tuning fork for enhancing the sensitivity of laser-induced thermoelastic spectroscopy. *Opt Express* **29**, 12195–12205 (2021).
41. Lou CG, Yang X, Li XT et al. Graphene-enhanced quartz tuning fork for laser-induced thermoelastic spectroscopy. *IEEE Sens J* **21**, 9819–9824 (2021).
42. Sun HY, Qiao SD, He Y et al. Parts-per-quadrillion level gas molecule detection: CO-LITES sensing. *Light Sci Appl* **14**, 180 (2025).
43. Wang RQ, Guan XY, Qiao SD et al. Ultrahigh sensitive LITES sensor based on a trilayer ultrathin perfect absorber coated T-head quartz tuning fork. *Laser Photonics Rev* **19**, 2402107 (2025).
44. Li SZ, Yuan YP, Shang ZJ et al. Ppb-level NH_3 photoacoustic sensor combining a hammer-shaped tuning fork and a 9.55 μm quantum cascade laser. *Photoacoustics* **33**, 100557 (2023).
45. Wu HP, Dong L, Zheng HD et al. Beat frequency quartz-enhanced photoacoustic spectroscopy for fast and calibration-free continuous trace-gas monitoring. *Nat Commun* **8**, 15331 (2017).
46. Ye WL, Liu WH, Luo WX et al. Calibration-free near-infrared methane sensor system based on BF-QEPAS. *Infrared Phys Technol* **133**, 104784 (2023).
47. Chen YJ, Ma HX, Qiao SD et al. Rapid ppb-Level methane detection based on quartz-enhanced photoacoustic spectroscopy. *Anal Chem* **97**, 6780–6787 (2025).
48. Liu XN, Qiao SD, He Y et al. High-stability and fast calibration-free temperature measurement based on light-induced thermoelastic spectroscopy. *Ultrafast Sci* **5**, 0083 (2025).
49. Lang ZT, Qiao SD, He Y et al. Disturbance-immune, fast response LITES gas sensor based on out-plane vibration mode employing micro Fabry-Perot cavity with heterodyne phase demodulation. *Sens Actuator B Chem* **419**, 136412 (2024).
50. Ma YF, Liu YH, He Y et al. Design of multipass cell with dense spot patterns and its performance in a light-induced thermoelastic spectroscopy-based methane sensor. *Light Adv Manuf* **6**, 1 (2025).
51. Li B, Feng CF, Wu HP et al. Calibration-free mid-infrared exhaled breath sensor based on BF-QEPAS for real-time ammonia measurements at ppb level. *Sens Actuator B Chem* **358**, 131510 (2022).
52. Lang ZT, Qiao SD, Ma YF. Fabry-Perot-based phase demodulation of heterodyne light-induced thermoelastic spectroscopy. *Light Adv Manuf* **4**, 23 (2023).
53. Človečko M, Grajcar M, Kupka M et al. High q value quartz tuning fork in vacuum as a potential thermometer in millikelvin temperature range. *J Low Temp Phys* **187**, 573–579 (2017).
54. Patimisco P, Sampaolo A, Mackowiak V et al. Loss mechanisms determining the quality factors in quartz tuning forks vibrating at the fundamental and first overtone modes. *IEEE Trans Ultrason Ferroelectr Freq Control* **65**, 1951–1957 (2018).
55. Zheng KY, Zheng CT, Hu LE et al. Near-infrared fiber-coupled off-axis cavity-enhanced thermoelastic spectroscopic sensor system for *in situ* multipoint ammonia leak monitoring. *IEEE Trans Instrum Meas* **70**, 9510409 (2021).
56. Ma YM, Sui X, Song F et al. Optical-domain modulation cancellation method for background-suppression and dual-gas detection in light-induced thermo-elastic spectroscopy. *Sens Actuator B Chem* **404**, 135168 (2024).

Acknowledgements

We are grateful for financial supports from the National Natural Science Foundation of China (Grant No. 62335006, 62275065, 624B2050, 62022032, and 62405078), Open Subject of Hebei Key Laboratory of Advanced Laser Technology and Equipment (HBKL-ALTE2025001), Heilongjiang Postdoctoral Fund (Grant No. LBH-Z23144 and LBH-Z24155), Natural Science Foundation of Heilongjiang Province (Grant No. LH2024F031), China Postdoctoral Science Foundation (Grant No. 2024M764172).

Author contributions

Yufei Ma and Ying He proposed the original idea and supervised the whole project. Yufei Ma revised the manuscript. Yuanzhi Wang performed the measurements and wrote the original manuscript. Shunda Qiao, Xiaonan Liu, Chu Zhang and Xiaoming Duan contributed to the discussions.

Competing interests

Yufei Ma serves as an Editor for the Journal, and no other author has reported any competing interests.